International Journal of Advanced Robotic Systems

OPEN ACCESS
ARTICLE

New Structural Design of a Compliant Gripper Based on the Scott-Russell Mechanism

Regular Paper

Wenji Ai[1] and Qingsong Xu[1]*

1 Department of Electromechanical Engineering, Faculty of Science and Technology, University of Macau, Taipa, Macau, China
*Corresponding author(s) E-mail: qsxu@umac.mo

Received 28 February 2014; Accepted 20 October 2014

DOI: 10.5772/59655

Abstract

This paper presents the structural design and analysis of a novel compliant gripper based on the Scott-Russell (SR) mechanism. The SR mechanism in combination with a parallelogram mechanism enables the achievement of a pure translation of the gripper tips, which is attractive for practical micromanipulation and microassembly applications. Unlike traditional pure-translation grippers, the reported SR-based gripper exhibits a simple structure as well as compact dimension because the in-plane space is fully used. The kinematics, statics and dynamics models of the gripper mechanism are established, and finite element analysis (FEA) simulations are carried out to verify the structure design. A prototype has been developed for experimental testing. The results not only demonstrate the feasibility of the proposed SR-based gripper design but also reveal a promising performance of the gripper when driven by piezoelectric stack actuators. Moreover, several variations of the gripper structure are presented as well.

Keywords Microgripper, mechanism design, Scott-Russell mechanism, FEA simulation

1. Introduction

Robotic micro- and nano-handling systems are important to realize the automated manipulation and assembly of objects in micro- and nanometre scales [1]. As a crucial device in micro-handling systems, the microgripper has attracted intensive attention from both academia and industry. According to the driving principle, various types of microgrippers have been previously proposed, including electrostatic [2], electrothermal [3] and piezoelectric microgrippers [4]. The piezoelectric actuator in particular is attractive thanks to its properties of quick response speed and ultrahigh positioning resolution [5, 6]. Therefore, a piezoelectric stack actuator (PSA) is employed for the drive in this research.

Concerning the structure design, a great number of microgrippers have been devised using compliant mechanisms. The reason lies in the fact that, as compared with traditional bearings, compliant mechanisms produce motion by making use of elastic deformation of the material. Hence, compliant mechanisms offer some advantages in terms of being backlash-free, friction-free and lubrication-free [7-11]. However, most of the existing microgrippers are constructed with two arms, which work based on rotary motion [12]. It is known that the reaction

force will appear at the contact point once the gripper tips make contact with the target object. When grasping some objects which have a curved surface, the reaction force may push the grasped object away from the gripper tips [13]. Hence, it is desirable to devise microgrippers whose tips provide a pure translational motion [14,15]. Nonetheless, the majority of parallel-motion grippers possess a complex structure [13,14], which complicates the analysis and fabrication procedures.

The motivation of the present research is to devise a new parallel-motion gripper with a simple structure. Specifically, a Scott-Russell (SR) mechanism and a parallelogram mechanism are adopted to design the structure of each gripper arm. The SR mechanism has been previously employed to develop micropositioning systems. For instance, two SR mechanisms were used in [16] to construct a two-level amplification of PSA stroke for the actuation of a micropositioner. An optimal design of the SR-based micropositioning mechanism was presented in [17] with the aim of achieving a maximum amplification of the small displacement of PSA. More recently, an SR mechanism was employed in [18] to devise an ultraprecision rotary micropositioning stage.However, limited effort has been made in the literature towards the extension of theSR mechanism to gripper design. In this work, a novel compliant gripper is devised based on an SR mechanism. It is shown that the employment of an SR mechanism facilitates the structural design of a gripper with a simple architecture. In comparison with traditional microgrippers, the proposed SR-based gripper allows the generation of a simple structure. Moreover, a compact dimension is achieved since the in-plane area has been fully used. The feasibility and performance of the proposed gripper is validated through both finite element analysis (FEA) simulations and experimental studies.

In the remainder of this paper, the mechanism design process of an SR-based compliant gripper is presented in Section 2. Section 3 and 4 presentkinematics modelling and stiffness, static and dynamic analyses, respectively. Section 5 describes the finiteelement analysis simulation which is conducted by ANSYS. Afterwards, a prototype microgripper is fabricated in Section 6 along with an account of open-loop performance. Discussions about the gripper performance and future work are reported in Section 7. Finally, Section8 concludes this paper.

2. Mechanism design

Figure 1 shows a CAD model of the devised compliant gripper. The gripper mechanism is designed using flexure hinges and is actuated by two piezoelectric stack actuators (PSA). Two preloading screws are used to adjust the preloading force between the PSA and gripper mechanism.

The gripper structure consists of two SR mechanisms, which are used to amplify the PSA stroke. The role of the two parallelogram mechanisms is to guide a pure translational motion of the two gripper tips. Moreover, a second-stage lever is added between the SR mechanism and the parallelogram mechanism to further amplify the displacement of each gripper arm. It is observed that the PSA is embedded within the gripper structure, which leads to a full use of the in-plane space and results in a compact size of the gripper dimension.

In this work, the flexure hinges are adopted as right-circular shapes. As illustrated in Figure 2, each flexure hinge can be considered as a revolute joint in combination with a torsional spring. As compared with other shapes, the right-circular hinge allows the achievement of the lower centre shift of the revolute joints. Based on the pseudo-rigid-body (PRB) model of the flexure mechanism, the displacement and stiffness model of the gripper mechanism are established as follows.

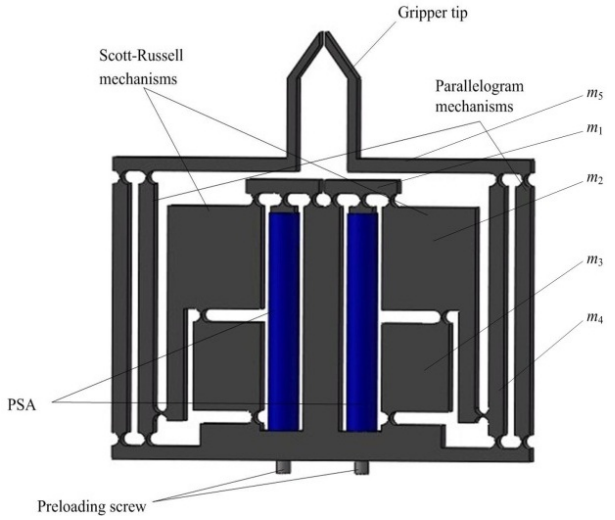

Figure 1. CAD model of a compliant gripper driven by two piezoelectric stack actuators (PSA)

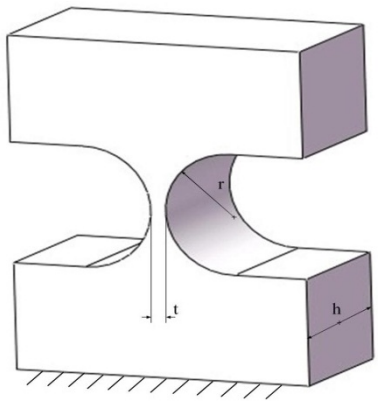

Figure 2. PRB model of right-circular flexure hinge

Scott-Russell mechanism: The schematic of a flexure hinge-based Scott-Russell mechanism is depicted in Figure 3. It is shown that O is a fixed pin joint, A is the input point to be driven by a PSA, and B is the output point.

Let $\overline{AC}=\overline{BC}=\overline{OC}=l$ and $\angle OAB=\theta$. Then, the coordinates of the output point B are:

$$x_B=\sqrt{4l^2-y_A^2} \tag{1}$$

$$y_B=0 \tag{2}$$

where y_A is the y-axis coordinate of point A.

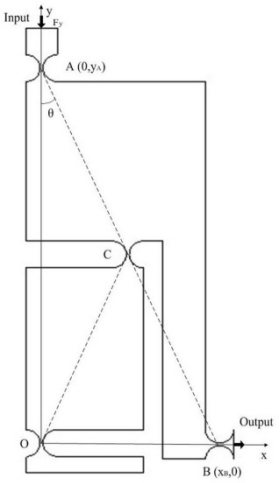

Figure 3. Schematic of a Scott-Russell mechanism using flexure hinges

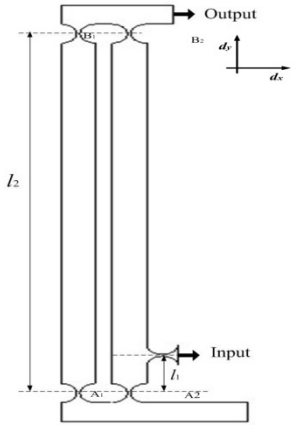

Figure 4. Parameters of the second-stage lever mechanism

Regarding a Scott-Russell mechanism under the condition of $\overline{AC}=\overline{BC}=\overline{OC}$, when the input point A moves along the y-axis with a displacement Δy_A, the output point B offers an exact straight-line translation Δx_B along the x-axis, i.e.,

$$x_B^2+y_A^2=(x_B+\Delta x_B)^2+(y_A+\Delta y_A)^2 \tag{3}$$

Solving (3) gives the expression of Δx_B as follows.

$$\Delta x_B=-x_B+\sqrt{x_B^2-2y_A\Delta y_A-\Delta y_A^2} \tag{4}$$

which indicates a nonlinear relationship between Δx_B and Δy_A.

As Δy_A approaches zero, i.e., $\Delta y_A \to 0$, the relation can be expressed in the form:

$$\eta_1=\frac{\Delta x_B}{\Delta y_A}\approx\frac{dx_B}{dy_A}=-\frac{y_A}{\sqrt{4l^2-y_A^2}}=-\frac{y_A}{x_B}=-\cot\theta \tag{5}$$

which is derived in view of (1).

From (5), it is found that a small displacement Δy_A along the y-axis will produce an amplified displacement $\Delta x_B=-\Delta y_A\cot\theta$ along the x-axis if $0<\theta<\pi/4$. The negative sign means that a decreased Δy_A will cause an increased Δx_B. Therefore, the Scott-Russell mechanism can be considered as a straight-line amplifying mechanism with a fixed amplification ratio in the case of small-motion applications.

Lever mechanism: The second-stage lever mechanism is depicted in Figure 4. It can be seen that the amplification ratio is

$$\eta_2=\frac{l_2}{l_1} \tag{6}$$

Therefore, the input-output displacement model of the gripper can be derived in consideration of (5) and (6):

$$A_s=\frac{x_{out}}{y_{in}}=\frac{l_2\cot\theta}{l_1} \tag{7}$$

which describes the ratio between the output and input displacements of the gripper tip.

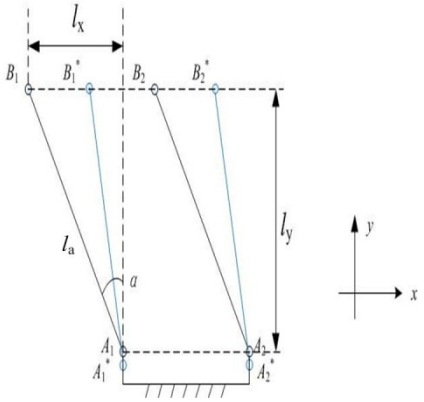

Figure 5. PRB model of the displacement amplifier and its parameters

3. Kinematics modelling

Given the input displacements (q_1 and q_2) of the two PSA actuators, the gripper output motion (d_{x1} and d_{x2}) and actuator input forces (F_{in1} and F_{in2}) can be calculated by the following kinematics and static sequations:

$$\begin{bmatrix} d_{x1} \\ d_{x2} \end{bmatrix} = \begin{bmatrix} A_s & 0 \\ 0 & A_s \end{bmatrix} \begin{bmatrix} q_1 \\ q_2 \end{bmatrix} \tag{8}$$

$$\begin{bmatrix} F_{in1} \\ F_{in2} \end{bmatrix} = \begin{bmatrix} K_{in} & 0 \\ 0 & K_{in} \end{bmatrix} \begin{bmatrix} q_1 \\ q_2 \end{bmatrix} \tag{9}$$

where A_s is the amplification ratio of the displacement amplifier; and K_{in} is the input or actuation stiffness of the gripper structure.

Through the aforementioned relations, the kinematics and statics problems are converted into the calculation of the amplification ratio and input stiffness of the structure, respectively. In this paper, a pseudo-rigid body (PRB) model of the structure is established by considering each flexure hinge as a 1-DOF revolute joint combined with a torsional spring with stiffness K_r. The stiffness equation of K_r with the best accuracy, as compared in [19], is adopted for calculation. Let F_x, Δx and Δy be the input force, input and output displacements, respectively.

First, only the compliances of the flexure hinges are considered in the PRB model. That is, it is assumed that each flexure hinge has 1-DOF rotational compliance arising from the rotational deformation, and other elements are all considered as rigid bodies.

The free-body diagram of one amplifier leg is shown in Figure 4 and Figure 5. Under the equilibrium status, the equation of moments at point A_1 can be derived as follows:

$$2M_r + \frac{F_x}{2} l_y = \frac{F_y}{2} l_x \tag{10}$$

with the moment

$$M_r = K_r = \Delta\alpha \tag{11}$$

where K_r and $\Delta\alpha$ denote the rotational stiffness and deformation of a notch hinge, respectively.

Differentiating both sides of the displacement relation $l_x = l_a \sin\alpha$ (where l_x and α are variable during the operation) with respect to time allows the generation of

$$\Delta y = l_a \cos\alpha \, \Delta\alpha = l_y \Delta\alpha \tag{12}$$

The translational stiffness K_1 of the compound parallelogram is contributed by the rotational stiffness of the four notch hinges, which can be calculated below based on the potential energy analysis

$$K_1 = \frac{K_r}{l_2^2} \tag{13}$$

where l_2 denotes the length of the limb leg as shown in Figure 4. Thus, the force F_x can be expressed as

$$F_x = K_1 \Delta y \tag{14}$$

Substituting (11), (12), (13) and (14) into (10) gives a relation between the variables F_x and $\Delta\alpha$ as follows:

$$\Delta\alpha = \frac{F_y l_x}{4K_r + \frac{K_r}{l_2^2} l_y^2} \tag{15}$$

Moreover, in view of the virtual work principle, an equation can be obtained

$$F_y \Delta x - F_x \Delta y = M_r \Delta\alpha \tag{16}$$

which implies that the work done by external forces is equal to that done by internal forces.

Inserting (11), (12), (14) and (15) into (16) leads to a relation of Fx and Δx alone, which further gives

$$\Delta x = \frac{F_y l_x^2}{K_r + \frac{K_r}{l_2^2} l_y^2} \tag{17}$$

In addition, the input stiffness can be calculated by (17)

$$K_{in} = \frac{K_r + \frac{K_r}{l_2^2} l_y^2}{l_x^2} \tag{18}$$

In this work, the main parameters of the designed compliant gripper are designed as shown in Table 1.

Parameter	Value	Unit
θ	24.6	°
l	39.0	mm
l_1	10.0	mm
l_2	90.0	mm
r	2.5	mm
t	0.5	mm
h	10.0	mm
l_y	7.5	mm

Table 1. Main parameters of the designed compliant gripper

4. Stiffness, stress and dynamics analysis

4.1 Stiffness and compliance analysis

The in-plane stiffness (K_x) of the gripper structure relates the in-plane external forces (F_x) applied on the gripper to the induced deflections (t_x). By contrast, as the inverse of

stiffness, the compliance ($C_x = 1/K_x$) reflects the linear deflection under the external load as follows:

$$t_x = C_x F_x \tag{19}$$

The compliance factor characterizes the output compliance (or output stiffness) of the structure suffering from external load.

Due to the symmetry of the left and right arms of the gripper structure, it can be deduced that $C_{x1} = C_{x2} = C_x$ in theory. In what follows, the output compliance C_x of the stage is derived with an x-axis external force F_x applied on the output platform.

$$\theta = t_x / 2l_a \tag{20}$$

The potential energies of the structure arise from the elastic deformations of the material, and are stored in the two limbs, which can be expressed in two different ways:

$$\frac{1}{2} K_x t_x^2 = 8 \times \frac{1}{2} K_r \theta_1^2 \tag{21}$$

where Kx is the output stiffness of the stage in x-axis direction, and Kr represents the rotational stiffness of each flexure hinge around the working axis.

Inserting (20) into (21) gives an expression for the output stiffness

$$K_x = \frac{2K_r}{l_a^2} \tag{22}$$

which implies that the output compliance is

$$C_x = \frac{l_a^2}{2K_r} \tag{23}$$

4.2 Stress and load capacity analysis

The in-plane load capacity F_x^{max} means the maximum external force that can be applied at the structure without causing the failure of the material.

For the in-plane operation, only the bending stress is taken into account to derive the load limit, because the axial tensile or compressive stress of the flexure hinge is far less than the maximum bending stress. For a flexure hinge bearing a bending moment around its rotation axis, the maximum angular displacement θ^{max} occurs when the maximum stress σ^{max}, which occurs at the outermost surface of the thinnest portion of the hinge, reaches the yield stress σ_y.

The relationship between the maximum bending stress and the maximum rotational deformation of the flexure hinge has been derived [20]:

$$\sigma^{max} = \frac{E(1+\eta)^{9/20}}{\eta^2 f(\eta)} \theta^{max} \tag{24}$$

where $\eta = t/2r$ is a dimensionless geometry factor; and $f(\eta)$ is a dimensionless compliance factor defined as

$$f(\eta) = \frac{1}{2\eta + \eta^2} \cdot \left[\frac{3 + 4\eta + \eta^2}{(1+\eta)(2\eta+\eta^2)} + \frac{6(1+\eta)}{(2\eta+\eta^2)^{3/2}} \tan^{-1}\left(\frac{2+\eta}{\eta}\right)^{1/2} \right] \tag{25}$$

Flexure hinges rotate with the same angle

$$\theta^{max} = t_x^{max} / 2l_a \tag{26}$$

where t_x^{max} is the corresponding maximum linear deformation of the stage. Under such a case, the maximum stress calculated by (32) should satisfy

$$\sigma^{max} = \frac{E(1+\eta)^{9/20}}{2l_a \eta^2 f(\eta)} t_x^{max} \le \sigma_y \tag{27}$$

which allows the derivation of

$$t_x^{max} \le \frac{2l_a \eta^2 f(\eta) \sigma_y}{E(1+\eta)^{9/20}} \tag{28}$$

Once the maximum deflection is generated earlier, the maximum in-plane load that can be supported by the structure is given by

$$F_x^{max} = K_x t_x^{max} \tag{29}$$

4.3 Dynamics and resonance frequency calculation

For the structure, considering the kinematics relation in (1), the coordinate vector of $\mathbf{q} = [q_1 q_2]^T$ is adopted to describe its in-plane motion. Then, the kinetic and potential energies of the stage stored in each gripper arm can be written in terms of the selected generalized coordinates.

Substituting the kinetic and potential energies into Lagrange's equation

$$\frac{d}{dt} \cdot \frac{\partial T}{\partial \dot{q}_i} - \frac{\partial T}{\partial q_i} + \frac{\partial V}{\partial q_i} = F_i \tag{30}$$

with i = 1 and 2, allows the generation of the dynamic equation describing a free motion of the stage

$$\mathbf{M}\ddot{q} + \mathbf{K}\mathbf{q} = 0 \tag{31}$$

where the 2 × 2 equivalent mass and stiffness matrices take on the diagonal forms **M** = diag{M} and **K** = diag{K}, respectively, along with

$$M = m_1 + \frac{1}{2}m_2 + \frac{1}{25}m_3 + \frac{88}{5}m_4 + 40m_5 \tag{32}$$

$$K = K_{in} \tag{33}$$

where the masses m_1 to m_5 are denoted in Figure 1.

Therefore, the in-plane resonance frequency of the stage can be obtained as

$$f_n = \frac{1}{2\pi}\sqrt{\frac{K}{M}} \tag{34}$$

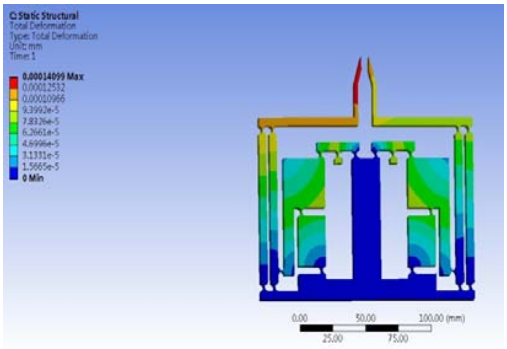

(a)

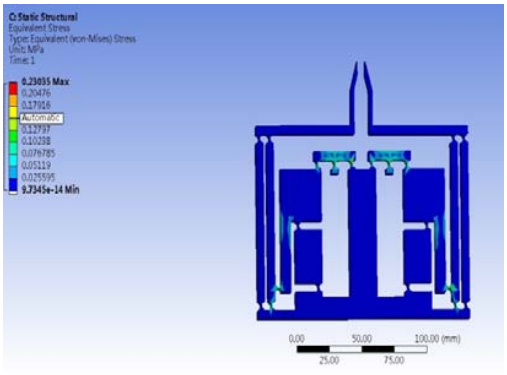

(b)

Figure 6. Static FEA simulation results. (a) Deformed shape; (b) stress distribution

5. Finite element analysis simulation

As a case study, an SR-based compliant gripper is designed with parameters as tabulated in Table 1. The material is chosen as Al-7075 alloy, its modular of elasticity is $E = 7.1\times 10^{11}$ Pa, Poisson's ratio $\mu = 0.31$, density $\rho = 2810 kg/m^3$, and yield strength [σ]=524MPa. The PSA is selected as model P-840.30 from PhysikInstrumente (PI) Gmbh& Co. KG. The actuator possesses a length of 68 mm, and provides a stroke of 45 μm and maximum pushing force of 1000 N. The kinematic model (7) predicts that the ratio between the output and input displacements are A_s = 13.1.

5.1 Static FEA simulation

First, the static structural FEA simulation has been carried out by applying an input force of 1 Non the input end of the gripper. The simulation result of the deformed shape is shown in Figure 6(a). After extracting the displacement values, the ratio between the output and input displacement is calculated as A_s =12.6.

As compared with the FEA result, the kinematic model overestimates 3.98% of the amplification ratio. The reason why the FEA result for the ratio is lower than that assessed by the analytical model arises from the deformations of the links between the flexure hinges. Only the bending deformations of the hinges are considered in the PRB model of the kinematic analysis, whereas other deformations exist as observed from the simulation results. Hence, a nonlinear modelling with consideration of all the deformations of the gripper mechanism will enhance the kinematic model's accuracy.

Additionally, the distribution of the equivalent stress is shown in Figure 6(b). It is observed that the maximum stress occurs at the hinge which links the SR mechanism and the lever mechanism.

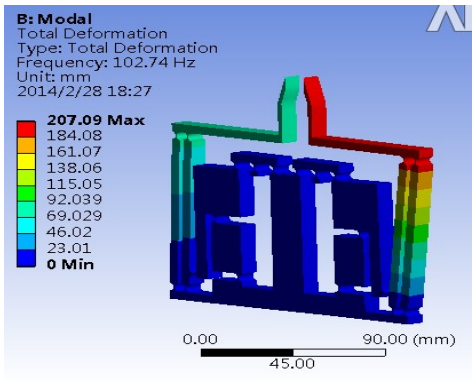

(a)

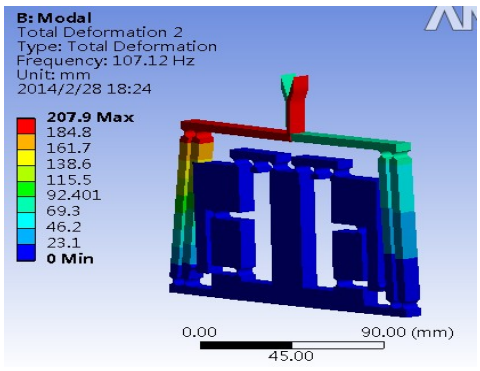

(b)

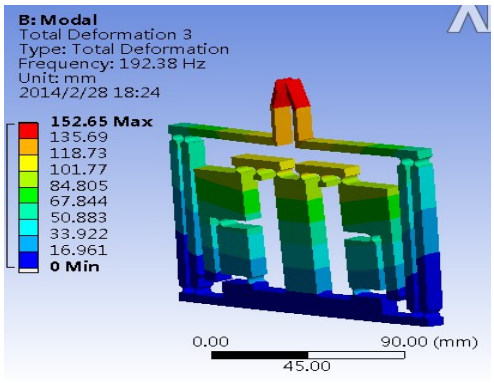

(c)

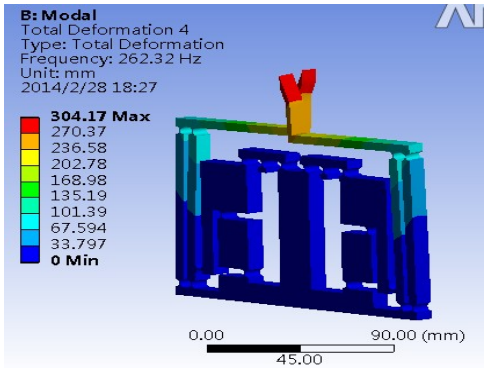

(d)

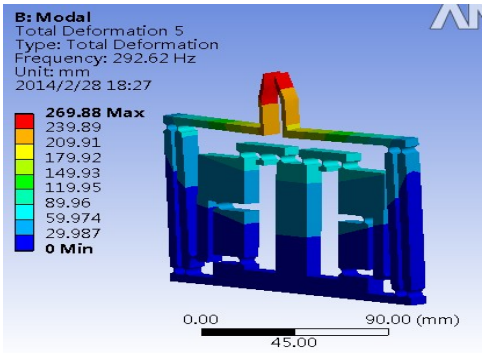

(e)

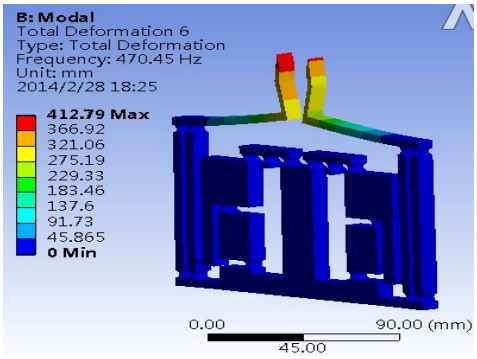

(f)

Figure 7. FEA simulation results of the first six mode shapes for the compliant gripper structure

5.2 Dynamic FEA simulation

Furthermore, modal FEA simulation has been conducted to examine the resonant mode frequencies and shapes of the gripper structure. The first six resonant mode shapes are shown in Figure 7, and the corresponding resonant frequencies are described in Table 2. It is seen that the first resonant mode at 102.74 Hz is attributed to the translation of the two parallelogram mechanisms along the same direction. The second mode at 107.12 Hz is contributed by the translation of the two parallelograms in opposite directions, which corresponds to the closing/opening working mode of the gripper tips. The third to fifth modes are caused by the out-of-plane deformations of the structure, while the sixth mode is induced by the in-plane bending deformation of one gripper arm.

Mode sequence	Frequency (Hz)
1	102.74
2	107.12
3	192.38
4	262.32
5	292.62
6	470.45

Table 2. The first six mode frequencies of the compliant gripper

The resonance frequency calculated by the dynamic model (34) is 108.83Hz. As compared to the FEA result, the dynamic model overestimates the resonance frequency with a deviation less than 6%, which validates the effectiveness of the derived model. It is observed from (34) that the resonance frequency of the structure can be magnified by increasing the input stiffness or reducing the equivalent mass of the stage. For instance, the material with a thinner thickness can be used for fabrication, and unnecessary mass of the moving parts can be removed to achieve a higher resonance frequency.

6. Prototype fabrication and experimental studies

6.1 Experimental setup

In this section, a fabricated prototype of the gripper structure is presented and preliminary open-loop testing is conducted to demonstrate the gripper performance.

A prototype microgripper is fabricated, which is graphically shown in Figure 8. The mechanism of the stage is fabricated by the wire-cutting process from Al-7075 alloy. Concerning the actuation, two 45μm-stroke PSAs (model P-840.3 produced by PhysikInstrumente Co., Ltd., see Table 3) are adopted to drive the stage. D/A board (NI-9215 DAC module) is employed to produce analogue voltages, which are then amplified by three-axis voltage amplifiers (model E-503.00 from PI GmbH&Co. KG.) to provide voltages of 0–100 V for the drives of the PSAs. In order to

measure the output displacements of the moving platform, a laser displacement sensor (LK-H055, from Keyence Corp.) is used. The analogue voltage outputs of the sensor signal conditioners are read simultaneously by a personal computer through a data acquisition (DAQ) board (NI-9263 ADC module). They are programmed using LABVIEW software and downloaded to a controller (NI cRIO-9022) to realize the real-time control, as shown in Figure 9.

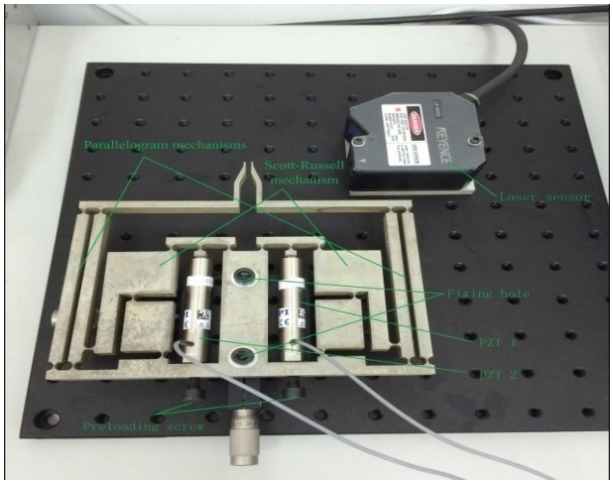

Figure 8. Prototype of the developed gripper

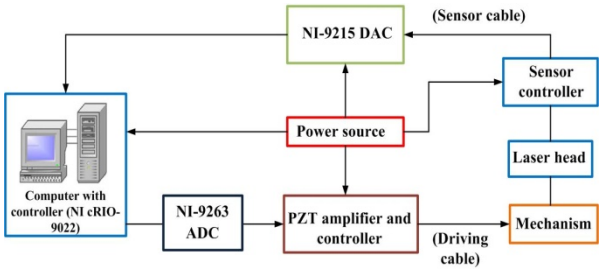

Figure 9. Hardware connection scheme

Item	Parameter
Size (mm)	Φ12*68
Weight (g)	46
Max. stroke (μm)	45
Max. thrust force (N)	1000
Output stiffness (N/μm)	19

Table 3. Specifications of the PSA actuator

In addition, each actuator is inserted into the mechanical amplifier and preloaded through the screw mounted at the tip of the actuator. This produces interference fits between the PSA and amplifier. Thus, no clearances exist during the operation due to elastic deformations of the material.

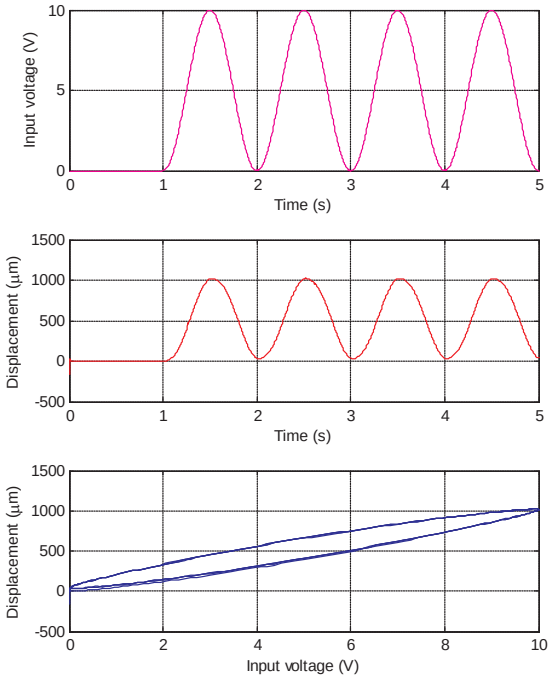

Figure 10. The output displacement and hysteresis characteristics of the gripper when PSA 1 is actuated with 1-Hz signal

6.2 Open-loop experimental test

First, the open-loop static properties of the structure are experimentally tested. A low-frequency 0.1 Hz sinusoidal voltage signal ranging from 0 to 10 V is provided, which is then amplified by the voltage amplifier and used to drive the PSA 1. With the open-loop voltage-driven strategy, the PSA exhibits nonlinearity which is mainly attributed to the hysteresis effects.

The hysteresis effect of the PSA influences the mechanism's motion accuracy. With different rates of input voltage signal to PSA 1, the dominant hysteresis loops for the x-axis motion are shown in Figure 10, which shows that the gripping range of each gripper tip is about 1000 μm. Similar results can be obtained when PSA 2 is driven.

In view of the stroke (45 μm) of the PSA, the amplification ratio of the stage can be determined as 22.2, which is larger than the FEA result. The reason for this is mainly the preloading effect of the PSA mounting. Because the two PSAs are inserted into the two mechanical amplifiers and preloaded using the screws, the preloading influences both the input displacement of PSA and the architecture parameters of the flexure mechanism. Since the PSA is inserted into the mechanical amplifier and preloaded using an adjusting screw, shown in Figure 8, the initial values for the parameters are changed. This produces interference fits between the PSA and amplifier. Hence, the ratio is greater than the nominal value.

In addition, the frequency response of the gripper is generated by a swept-sine approach. From Figure 11, it is found that the natural frequency of the mechanism is about 70 Hz, which is smaller than the FEA result. The reason is that the two PSAs increase the mass of the mechanism.

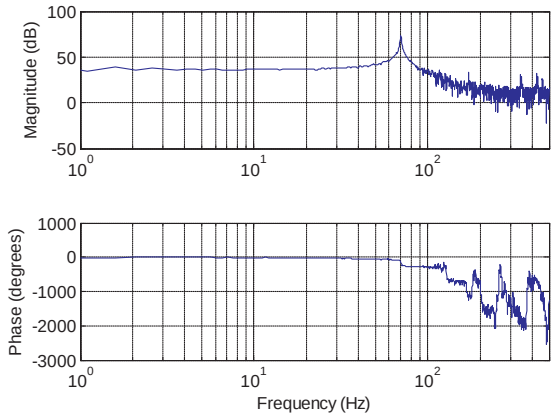

Figure 11. Bode diagram of the model with varioussampling times

7. Discussion and future work

The conducted experimental studies verified the feasibility of the proposed gripper design based on the SR mechanism. The accuracy of the kinematic model can be enhanced by considering all of the deformations of the structure. Besides this, the resonant frequency of 70 Hz may be increased by implementing an optimal design of the stage parameters.

In addition, the gripper can also be designed using multiple tips, as illustrated in Figure 12. It is found that the three tips of the gripper are driven separately to grasp the micro-object, which renders a more dexterous and reliable micromanipulation operation. By employing one gripper arm as a basic module, a modular gripper can be easily developed using more gripper tips.

In order to realize a microscale positioning, the piezoelectric hysteresis effects will be compensated by a controller. Both the error sources and piezoelectric hysteresis affect the open-loop positioning accuracy of the micropositioning stage. In future work, a controller design should be carried out to remedy the above shortcomings in order to realize a microscale manipulation.

Furthermore, in targeting a micromanipulation and microassembly application, a force control of the gripper tips is crucial to guarantee a safe gripping of fragile objects [8, 19]. In the future, force sensors will be employed to measure the grasp force of the gripper, and position/force control will be implemented to realize an appropriate position and force control strategy. The feasibility of the proposed gripper will be demonstrated by gripping different objects with controlled grasp force.

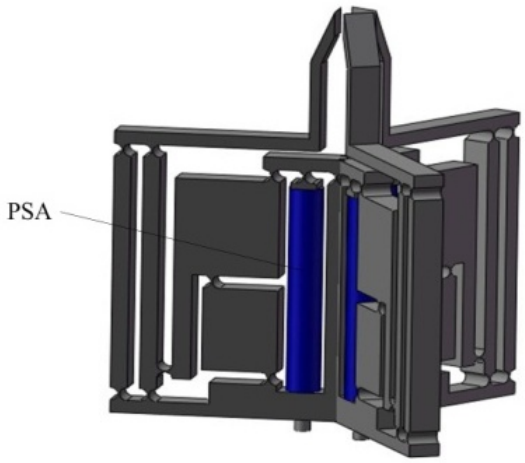

Figure 12. CAD model of a modular compliant gripper with the three tips driven separately

8. Conclusion

A new compliant gripper based on a Scott-Russell mechanism is proposed in this paper to amplify the PSA input displacement and to achieve a parallel motion of the gripper tips. An analytical model is established to facilitate the design of gripping range, and the model is verified with finite element analysis. Simulation results reveal that the gripper arms allow a pure translational motion. In addition, the gripper structure possesses a high resonance frequency which enables a rapid response. A prototype has been fabricated and experimental investigations have been performed accordingly. In comparison with traditional microgrippers, the proposed Scott-Russell based gripper allows the generation of a simpler structure. A compact dimension is achieved since the in-plane area has been fully used. It is found that the developed gripper exhibits a resonance frequency of 70 Hz and a large displacement amplification ratio of 22.2. In the future, force sensing/control will be realized to guarantee a desired microhandling of fragile objects in subsequent work.

9. Acknowledgements

The work was supported by the Macao Science and Technology Development Fund under Grant No.: 070/2012/A3 and the Research Committee of the University of Macau under Grant Nos.: MYRG083(L1-Y2)-FST12-XQS and MYRG078 (Y1-L2)-FST13-XQS.

10. References

[1] Fatikow S, Eichorn V (2008) Nanohandling automation: Trends and current developments. Proc. Inst. Mech. Eng. Part C-J. Mech. Eng. Sci. 222: 1353-1369.

[2] Beyeler F, Neild A, Oberti S, Bell DJ, Sun Y, Dual J, Nelson BJ et al. (2007) Monolithically fabricated microgripper with integrated force sensor for manipulating microobjects and biological cells

aligned in an ultrasonic field. J. Microelectromech. Syst. 16: 7-15.

[3] Kim K, Liu X, Zhang Y, Sun Y et al. (2008) Nanonewton fore-controlled manipulation of biological cells using a monolithic MEMS microgripper with two-axis force feedback. J. Micromech. Microeng. 18: 055013.

[4] Menciassi A, Eisinberg A, Carrozza MC, Dario P et al. (2003) Force sensing microinstrument for measuring tissue properties and pulse in microsurgery. IEEE/ASME Trans. Mechatron. 8: 10-17.

[5] Zhang G, Zhang C, GuJ et al. (2012) A memory-based hysteresis model in piezoelectric actuators. Journal of Control Science and Engineering.2012: 7.

[6] Xu Q (2013) Identification and compensation of piezoelectric hysteresis without modeling hysteresis inverse. IEEE Trans. Ind. Electron. 60: 3927-3937.

[7] Kemper M (2004) Development of a tactile low-cost microgripper with integrated force sensor. IEEE Trans. Robot. pp.1461-1466.

[8] Xu Q (2012) New flexure parallel–kinematic micropositioning system with large workspace. IEEE Trans. Robot. 28: 478-491.

[9] Nah S, Zhong Z (2007) A microgripper using piezoelectric actuation for micro-object manipulation. Sens. Actuator A-Phys. 133: 218-224.

[10] Xu Q (2014) Design and development of a compact flexure-based XY precision positioning system with centimeter range. IEEE Trans. Ind. Electron. 61: 893-903.

[11] Zubir M, Shirinzadeh B, Tian Y et al. (2009) Development of a novel flexure-based microgripper for high precision micro-object manipulation. Sens. Actuator A-Phys. 150: 257-266.

[12] Xu Q (2013) A new compliant microgripper with integrated position and force sensing. In: Proc. IEEE/ASME Int. Conf. on Advanced Intelligent Mechatronics. pp. 591-596.

[13] Keoschkerjan R, Wurmus H (2002) A novel microgripper with parallel movement of gripping arms. In: Proc. of 8th Int. Conf. on New Actuators. pp. 321-324.

[14] Zubir M, Shirinzadeh B, Tian Y et al. (2009) Development of a novel flexure-based microgripper. Precis. Eng. 33: 362-370.

[15] Xu Q (2012) Mechanism design and analysis of a novel 2-dof compliant modular microgripper. In: Proc. 7th IEEE Conf. on Industrial Electronics and Applications. pp. 1966-1971.

[16] Chang S, Chang B (1998) A precision piezodriven-micropositioner mechanism with large travel range. Rev. Sci. Instrum. 69: 1785-1791.

[17] Ha J, Kuang Y, Hu S, Fung R et al. (2006) Optimal design of a micro-positioning Scott-Russell mechanism by Taguchi method. Sens. Actuator A-Phys. 125: 565-572.

[18] Hwang D, Byun J, Jeong J, Lee M et al. (2011) Robust design and performance verification of an in-plane xyθ micropositioning stage. IEEE Trans. Nantechnol. 10: 1412-1423.

[19] Yong Y, Lu T, Handley D (2008) Review of circular flexure hinge design equations and derivation of empirical formulations. Precis. Eng. 32: 63-70.

[20] Smith S (2000) Flexures: Elements of Elastic Mechanisms. New York: Gordon and Breach.

[21] Xu Q (2012) Precision position/force interaction control of a piezoelectric multimorphmicrogripper for microassembly. IEEE Trans. Autom. Sci. Eng. 10: 503-514.